www.vbripress.com, www.amlett.com, DOI: 10.5185/amlett.2011.3233 Published online by the VBRI press in 2011

Microstructure, phase formations and optical bands in nanostructured alumina

Jitendra Gangwar[a,b], Kajal Kumar Dey[a], Komal[a], Praveen[a], Surya Kant Tripathi[b], Avanish Kumar Srivastava[a*]

[a]*National Physical Laboratory, Council of Scientific and Industrial Research, Dr. K. S. Krishnan Road, New Delhi 110012, India*
[b]*Department of Physics, Panjab University, Chandigarh 160014, India*

[*]Corresponding author. Tel: (91) 11 45609308; Fax: (91) 11 45609310; E-mail: aks@nplindia.ernet.in, avanish.aks555@gmail.com

Received: 05 March 2011, Revised: 28 May 2011 and Accepted: 01 June 2011

ABSTRACT

We report the synthesis of nano-scaled alumina of varied dimensions through a novel optimized processing of aluminum nitrate. The X-ray diffractometry confirmed the formation of α- and γ- phases of alumina particles in the nano region, depending on the annealing conditions during processing. Subsequently, a detailed microscopic investigation revealed the morphological alterations and crystallographic information even at lattice scale. The presence of different bonds and band energies were investigated by employing infra-red and photoluminescence spectrometry, respectively. The evolution of fascinating microstructure, phase formations and optical bands has been presented and discussed to elucidate the systematic evolution of different crystalline phases (α and γ) from an amorphous alumina with increased annealing temperature.

Keywords: Alumina; high resolution electron microscopy; α- and γ- phases; optical bands.

A. K. Srivastava did Ph.D. at IISc Bangalore, (Metallurgy), M.Tech. at IIT, Kanpur (Materials Science), M.Sc. at IIT, Roorkee (Physics). He has collaborations with IISc Bangalore, BHU Varanasi, IIT Delhi, IIT Kanpur, University of Paris (France), University of Reims (France), Technical University Darmstadt (Germany), University of Arkansas (USA), University of Okayama (Japan) and POSTECH (South Korea). He has about 110 publications in highly reputed international journals.

J. Gangwar did M.Sc. in Physics at MJP-Rohilkhand. Registered at the Panjab University, Chandigarh, he is pursuing his Ph.D from National Physical Laboratory, New Delhi in the area of synthesis and characterization of oxide nanostructures.

S.K. Tripathi is working as Associate Professor in the Department of Physics, Panjab University, Chandigarh. He has keen interest on the electrical, optical, thermal and structural measurements of the materials like nanomaterials, nanocomposites, oxides, organic materials, phase change materials, glasses etc in the thin film forms.

Introduction

In an era dominated by efforts towards miniaturization of electronic and mechanical devices, structures with a size in the nanometer (10^{-9} m) realm have perked up intensive, worldwide research activities. Various inorganic oxide nanostructures, both pure and doped have been subjected to extensive research activities, not only because of their wide range of applications but also because of the intrigue, they present with their typical properties [**1-9**]. Among such nanostructures, various amorphous, poriferous and 1-D shaped nanostructures of alumina make for engaging studies because of the multi-functionality that can be consorted with their respective peculiar shapes and surface lineaments **[10, 11]**. These tremendous possibility for potential applications though, requires cautious mastery over the skill to tailor the shape and size, as well as low cost and hazard free methods for mass production – both great challenges for either of bottom up and top down access to such nanostructures.

Alumina or aluminium oxide nanostructures are such a breed of materials which, because of its rich array of existing and potential applications require smooth and highly effective synthetic strategy. Alumina is known to exist in a number of metastable polymorphs in addition to the thermodynamically stable α-Al_2O_3 or corundum form.

Much of the Greek alphabets have been exhausted in labeling these phases (e.g. γ, δ, η, θ, κ, β, χ etc), among which γ-alumina is an extremely important material in catalytic surface activity [**12-17**]. Corundum nanopowder has considerable potential for a wide range of applications which includes high strength materials, electronic ceramics, catalyst and electrochemical sensors [**18, 19**]. High quality nanocrystals of corundum are also used as electronic substrates, bearing in watches and other fine precision equipments [**20**] and abrasive materials [**21**]. Because of its large band gap (8 eV) alumina serves as a tunneling barrier for magnetic sensors (which are based on the tunneling magnetoresistance effect) and for organic transistors **[22]**. Nano α-alumina can be used as a microwave dielectric material for lowering the sintering temperature **[23]**. Alumina has also got vital applications in biomedical field as nano alumina fiber has been used for the separation of virus and protein because of its rapid dynamic response for absorbing bacteria, virus and nucleic acids from biological solutions **[24].** Because of its high compressive strengths, very low co-efficient of friction, negligible wear rate and extreme chemical inertness in physiological environment, alumina has been well exploited in the construction of orthopedic joints such as hip-joint or knee joint **[25]**. In the past various synthesis methods, both physical and chemical, have been employed to synthesize nanoscaled alumina nanoparticles, e.g. spray pyrolysis [**26,27**], precipitation [**28**], combustion synthesis [**29**], sol-gel [**30**], hydrothermal [**31**], spark plasma sintering [**32**] etc. Synthesis of alumina ultrafine powders generally results in a mixture of phases (θ, γ, δ) and these phases transform to the more stable phases of α-alumina by heating at a high temperature. As a result it is quite difficult to formulate a processing route in order to obtain a single phase such as γ-alumina.

In this work, nano-sized alumina has been produced by using a simple novel processing method of annealing the saturated solutions of aluminum nitrate. The synthesis procedure was carried out without the usage of any costly templates or chemicals and without using any complicated instrumentations and even though, the method was extremely simple, the yield of the product alumina was remarkably high and suitable for industry level manufacturing. The resulting ultrafine powder of alumina was studied with respect to its morphological and band energies. The phase transformation with annealing temperatures was observed and efforts were made to co-relate with the nano-scaled morphological characteristics.

Experimental

The processing of nano alumina particles was carried out by taking saturated aqueous solution of aluminum nitrate nonahydrate, which was transformed to the gel form by heating it for 30 minutes at 100^0C. Subsequently the gel was annealed at a muffle furnace for three different temperatures of 400, 800 and 1000 ^{0}C for 2 hours each. After annealing the obtained white powder was used for further characterization. In these experiments, aluminum nitrate nonahydrate [Al $(NO_3)_3.9H_2O$] (99.9%) of analytical grade was procured from M/S alfa aesar and was used without any further purification.

The crystallographic phase identification and the purity determination of the obtained samples were carried out by X-ray diffraction (XRD, Bruker AXS D8 Advance X-ray Diffractometer) using monochromatized Cu-kα radiation (λ=1.54059Å) and scanning in 2θ range from 20^0 to 80^0. The FTIR spectra were recorded with a single beam Perkin Elmer instrument (Spectra BX-500) FT-IR Model spectrometer. The morphological characteristics and sizes of the synthesized samples were revealed by the scanning electron microscopy images recorded on a Zeiss EVO MA-10 SEM equipped with an energy dispersive spectrometer (OXFORD INCA ENERGY 250), which assisted in the elemental analysis of the sample. Further the surface topography of powder particles was analyzed by scanning helium ion microscopy (HIM, model: Zeiss ORION). The three dimensional surface topography was determined using Atomic Force Microscopy. Microstructural characterization at high magnifications and reciprocal space analysis was performed using a high resolution transmission electron microscope (HR-TEM: FEI Tecnai G2 F30 STWN at 300 keV). The optical properties of the powdered samples were investigated by photoluminescence spectroscopy using a Perkin-Elmer LS-55 luminescence spectrometer (Xe source) and the UV-Vis spectroscopy of the samples were carried out using the Perkin-Elmer Lambda 25 spectrometer.

Results and discussion

Crystallographic phase identification

Fig. 1 shows the XRD patterns of the nanoparticles synthesized under three different processing conditions. Pattern `a' corresponds to the samples obtained after annealing the precursor at 400 ^{0}C for two hours. From the pattern it is clearly observed that the sample is largely amorphous and thus no clear peak was visible. But to authenticate the formation of alumina particles under this condition the corresponding EDS pattern is given in (**Fig. 2**) The EDS analysis reveals the weight content of Al and O to be 54.54% and 45.46% respectively, giving the atomic content ratio Al/O of 41.57/58.43; almost 2/3, which verifies the formation of alumina particles to a large extent, since no other element was detected. There is also the minor possibility of some phase other than alumina being present in the sample; however that requires further experimental probe and analysis. Pattern `b' corresponds to the samples obtained after annealing the precursor at 800 ^{0}C for two hours. Unlike the samples synthesized at 400 ^{0}C, this sample clearly shows crystalline nature and simultaneous presence of two different alumina phases; α and γ. The visible diffraction intensities corresponding to the α phase agrees well with the peaks of rhombohedral crystal structure of alumina (JCPDS No.46-1212) with unit cell parameters of a = 0.47587 nm, c = 1.29929 nm. The diffraction intensities corresponding to the γ phase were in agreement with the peaks of cubic crystal system (JCPDS No.50-0741) and unit cell parameter of a = 0.7939 nm. Pattern `c' corresponds to the samples obtained after annealing the precursor at 1000 ^{0}C for two hours. It reveals

the presence of α-phase only in the corresponding sample. So the XRD patterns obviously indicate the transformation from γ to α at a high temperature and from amorphous to crystalline material at a lower temperature.

The FT-IR investigations (**Fig. 3**) also assist us in determining the phase and its transformation nature to some extent. The presence of peaks 2914 and 3498 cm^{-1} in the first two samples could be attributed to the presence of –OH species, indicating the presence of Al-OH bonds in these samples. The absorbance peak at 1456 cm^{-1}, for the sample annealed at 400 ^{0}C corresponds to Al=O bond stretching [**27**]. The other two peaks may have their origin in adsorption of atmospheric CO_2 and other impurities. For the second sample (annealed at 800 ^{0}C), the peaks at 584 and 868 cm^{-1} can be attributed to Al-O-Al bending mode and Al-O stretching mode respectively [**32**]. The other peaks may be due to some unwanted impurities in the sample. For the third sample (annealed at 1000 ^{0}C) there is only one prominent intense sharp peak at 513 cm^{-1}, which corresponds to O-Al-O bending mode. The FT-IR study tends to suggest the formation of pure alumina sample occurs through the intermediate formation of a hydroxy species. The plausible chemical reaction that occur leading to formation of alumina is given below:

$$2\ Al(NO_3)_3.9H_2O \rightarrow 2\ Al(OH)_3 + 6\ HNO_3 + 3H_2O$$

$$Al(OH)_3 \rightarrow AlOOH$$

$$AlOOH \rightarrow Al_2O_3 + H_2O$$

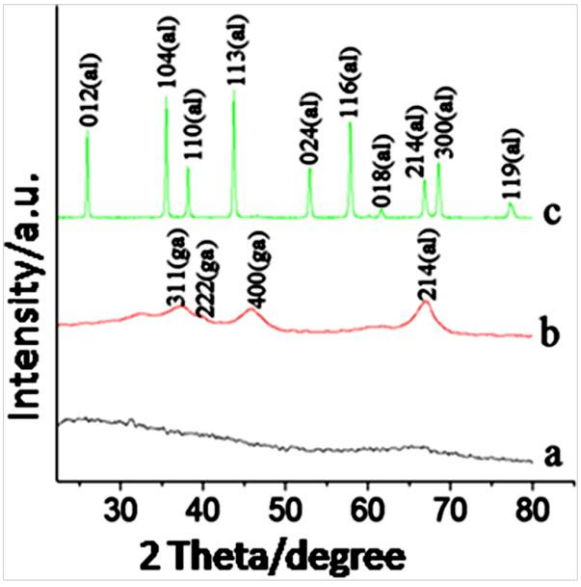

Fig. 1. XRD patterns of alumina nanoparticles synthesized by sol-gel method at different annealing temperature; a) 400 ^{0}C, b) 800 ^{0}C and c) 1000 ^{0}C. al: alpha (α) phase; ga: gamma (γ) phase.

Table 1 and **2** gives the crystallite sizes of the synthesized nanoparticles (corresponding to annealing temperature of 800 ^{0}C and 1000 ^{0}C), calculated from the XRD patterns using the Debye-Scherrer equation:

$$D = K\lambda/\beta\cos\theta$$

Crystallite size calculation for the first sample (annealed at 400^{0}C) could not be performed owing to the absence of any proper peak in the XRD pattern of that sample. From the two tables it is pretty clear that the crystallite sizes of the nanoparticles show an upward trend in their dimensionalities as the annealing temperature was increased from 800 to 1000 ^{0}C indicating a fascinating crystal transformation and regeneration process along with phase transmutation.

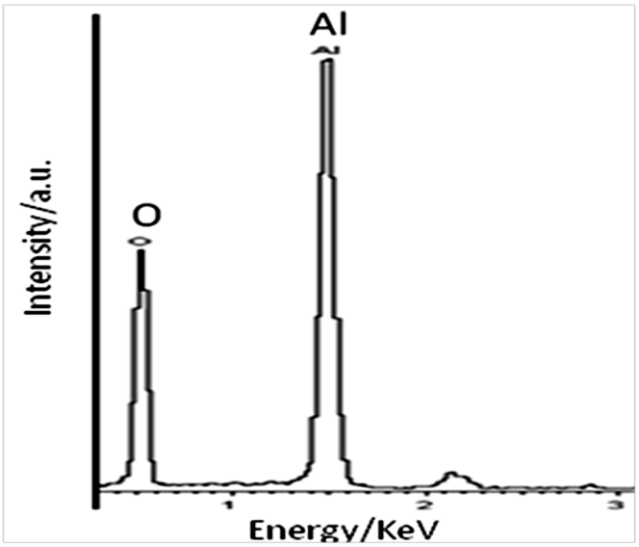

Fig. 2. EDS pattern of the alumina nanoparticles processed by annealing the precursor at 400 ^{0}C.

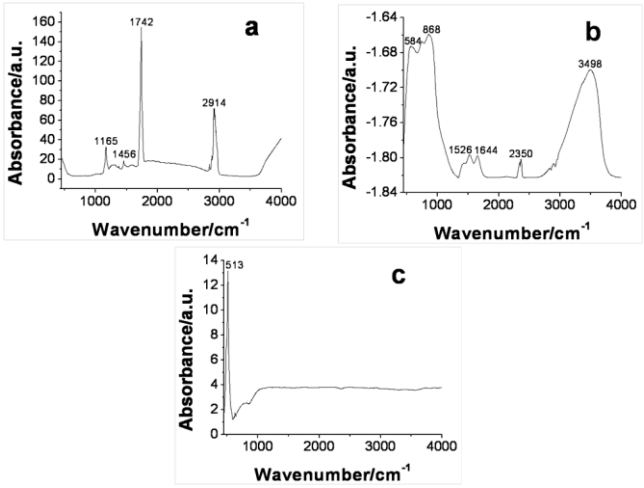

Fig. 3. FT-IR spectra of alumina samples synthesized by annealing the precursor at different temperature; a) 400 ^{0}C, b) 800 ^{0}C and c) 1000 ^{0}C

Microstructural characterization

Fig. 4 shows the SEM micrographs of the as synthesized nanoparticles under different reaction conditions. (**Fig. 4 (a)**) shows the micrographs of the alumina particles synthesized annealing the gel at 400 ^{0}C. Several scattered micro-pores (pores of dimension in the micrometer) are clearly visible from these images and the formation of grain like particles is also observed (**Fig. 4a (inset)**). The

presence of porosity in the sample indicates that this material can be extremely useful in catalytic applications.

Table 1. Crystallite size at different 2 theta values for the sample annealed at 800 ^{0}C.

2 theta Value (degrees)	Phase	d-value Å	(h k l)	FWHM (β)	Intensity Count	Crystallite Size(nm)
37.36	γ	2.407	3 1 1	1.96	539.48	4
39.88	γ	2.265	2 2 2	1.95	508.83	4
45.84	γ	1.980	4 0 0	1.96	529.63	4
67.10	α	1.400	2 1 4	1.83	551.52	5

Table 2. Crystallite size at different 2 theta values for sample annealed at 1000 ^{0}C.

2 theta Value (degrees)	Phase	d-value Å	(h k l)	FWHM (β)	Intensity Count	Crystallite Size (nm)
25.90	α	3.501	0 1 2	0.19	1073.48	43
35.52	α	2.525	1 0 4	0.20	1163.22	42
38.18	α	2.407	1 1 0	0.21	962.96	40
43.76	α	2.082	1 1 3	0.22	1199.32	39
52.92	α	1.750	0 2 4	0.26	938.88	34
57.98	α	1.604	1 1 6	0.28	1068.65	32
61.60	α	1.510	0 1 8	0.36	833.83	26
66.90	α	1.400	2 1 4	0.30	923.57	32
68.50	α	1.375	3 0 0	0.31	972.81	31
77.18	α	1.242	1 1 9	0.54	852.44	19

As we study the SEM micrographs of the sample synthesized by annealing the gel at 800 ^{0}C (**Fig. 4b**), the formation of bigger grain like particles are observed. Interestingly the size of the pores also witnessed an increment. This annealing temperature dependent size variation of the pores can be utilized in selective catalysis where the size of the pores plays an important role in deciding the catalytic activity of the material. The SEM micrographs of the samples synthesized annealing the gel at a temperature of 1000 ^{0}C (**Fig. 4 (c, d)**), although doesn't bear witness for much of a microstructural variation from the previous sample, but it clearly shows the paucity of pores on the surface. Although on increasing annealing temperature the size and density of pores are conventionally supposed to go up, but here this peculiar anomalous behavior can be rationalized keeping in mind that this sample is composed entirely of the α phase of the alumina, whereas the other phase was a concoction of both α and γ, as has been confirmed by the XRD patterns of the respective samples and the porous structure of alumina is normally associated with the γ phase of this ceramic material. Although the porous structure somewhat got disappeared, formation of nano-channels and grooves are observed (**Fig. 4d**), which defines another intriguing dimension of this sample.

The surface topographical characteristics of the sample were subjected to extended exploration employing helium ion microscope. (**Fig. 5**) shows the HIM images of the samples corresponding to annealing temperatures of 800 ^{0}C (**Fig. 5a**) and 1000 ^{0}C (**Fig. 5b**). The first one, which is comprised largely of the γ phase of alumina, shows uniform cellular surface topography. The second one which is comprised of only the α phase of alumina, shows a tendency of grain growth and a globular surface topography. The grain like structures of this sample is further confirmed by the AFM images of this sample (**Fig. 6**). The 2D image of the sample (**Fig. 6a)** reveals the globular grain like morphology; the inset provides indication of cluster formation. whereas, the 3D image (**Fig. 6b**) shows the presence of slight porosity in the sample; reaffirming the fact that by annealing at higher temperature the morphology of the sample along with its phase composition takes a new identity.

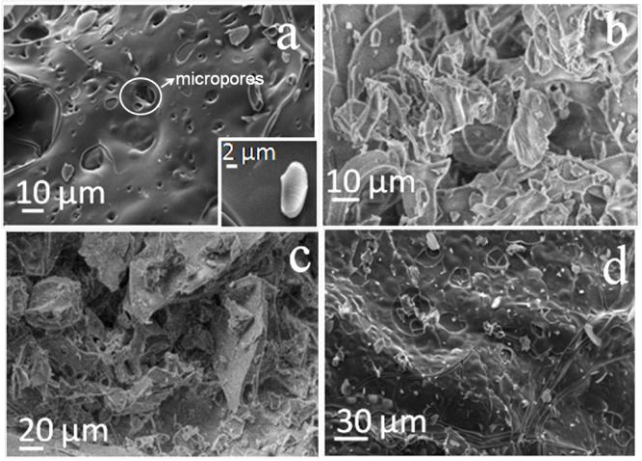

Fig. 4. SEM micrographs of alumina nanoparticles processed under different annealing temperatures recorded in a) 400 ^{0}C, b) 800 ^{0}C, c and d) 1000 ^{0}C. The inset image in a shows an isolated grain-like particle.

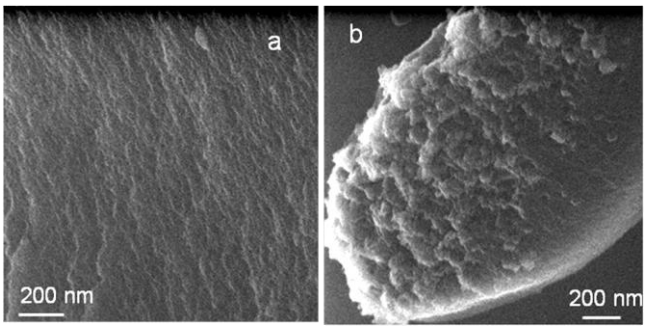

Fig. 5. Helium Ion Microscope images of the alumina samples synthesized at two different annealing temperatures; a) sample corresponding to annealing temperature of 800 ^{0}C, showing a cellular surface topography, b) sample corresponding to annealing temperature of 1000 ^{0}C, revealing a globular superficial topography.

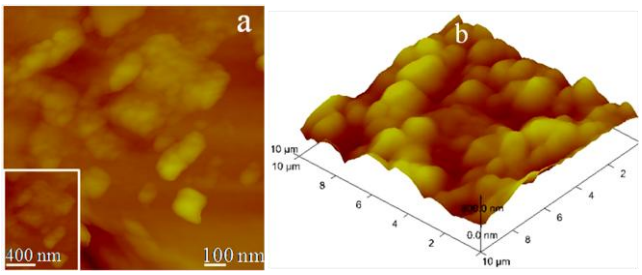

Fig. 6. AFM micrographs of the alumina samples synthesized at 1000 ^{0}C a) 2D and b) 3D representation. Inset in a shows low magnification image.

Fig. 7-9 shows the HRTEM images of the three alumina samples synthesized by annealing the precursor at three different temperatures. The HRTEM image of the sample processed by annealing the precursor at 400 ^{0}C

(**Fig. 7**) shows the featureless amorphous-structure of the sample. The featureless contrast confirms the fact that was already established from the XRD data of the corresponding sample. The SAED (inset in **Fig. 7**) also, exhibits a diffused pattern further corroborating the amorphous nature of the sample. The HRTEM micrograph of the sample corresponding to the annealing temperature of 800oC reveals the formation of ultra-fine nanoparticles (**Fig. 8a**) with the polycrystalline nature of the sample being confirmed by the ring pattern of the SAED (displayed as inset). Expectedly, the ring pattern also exhibits the simultaneous presence of α and γ phase of alumina (with ring 1 and 4 corresponding to α phase, ring 2 and 3 corresponding to γ phase) further strengthening the facts already obtained from XRD data. However, from the microstructure, it is difficult to distinguish between the α- and γ- phases. In this figure we could observe several randomly oriented crystallites. Most of these crystallites are abutting each other and forming an ultrafine network structure of alumina particles. The simultaneous existence of vast featureless area in the image also denotes that the sample contains some amorphosity.

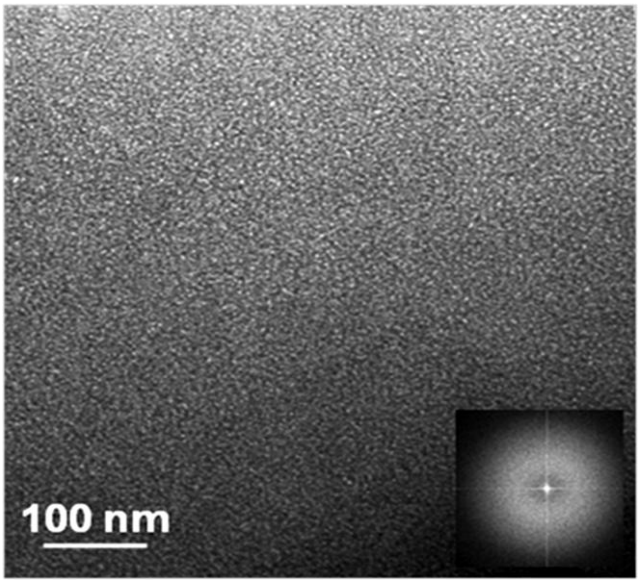

Fig. 7. HRTEM image of the alumina nanoparticles obtained by annealing the precursor at 400^{0}C . Inset shows corresponding SAED.

The lattice fringe image (**Fig. 8b**) exhibits the regular spacing of the clear lattice plane to be 0.204 nm which corresponds well to the (400) lattice plane of the γ-phase of alumina. The atomic scale imaging **(Fig. 8b)** of the nanocrystallites were carried out from a small region as indicated by an arrow in **Fig. 8a**. The HRTEM micrograph of the third sample, corresponding to annealing temperature of 1000 ^{0}C, shows the formation of larger grain like particles (**Fig. 9a**), the clear lattice plane spacing (**Fig. 9b**) of 0.26 nm matches well with the lattice plane (104) of the α-phase of alumina. So the HRTEM images prove to be compatible with the data that we obtained from the XRD measurements. Starting from the transformation from amorphous to crystalline state of the materials and also the phase transubstantiation between γ and α, both these phenomena has been well established through the HRTEM studies.

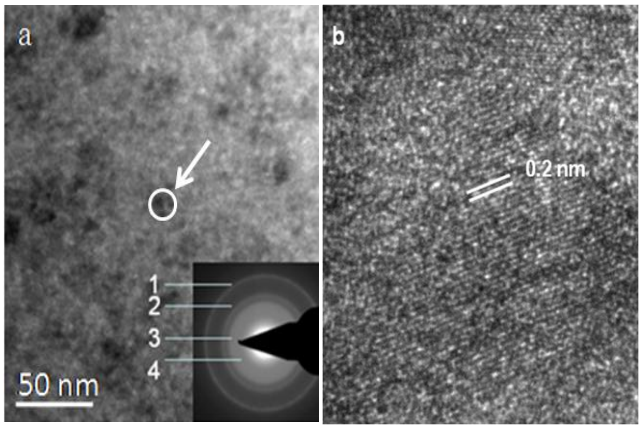

Fig. 8. HRTEM image of the nano alumina processed at 800 ^{0}C showing a) particles along with the SAED pattern, b) lattice scale fringes. SAED pattern (inset in a) marked for different rings; 1: d spacing 0.14nm (214 lattice plane of α phase), 2: d spacing 0.2nm (400 lattice plane of γ Phase), 3: d spacing 0.25nm (311 lattice plane of γ phase), 4: d spacing of 0.32nm (012 lattice plane of α phase).

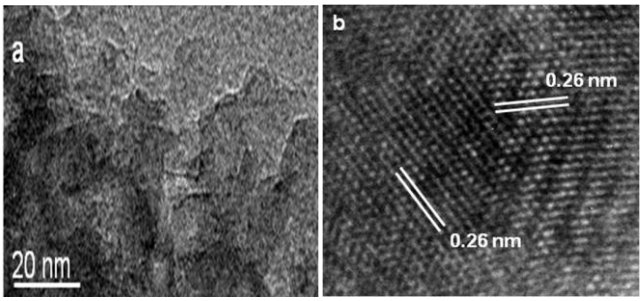

Fig. 9. HRTEM images of the alumina sample processed at 1000 ^{0}C showing a) the presence of grain like particles, b) the lattice scale fringes.

Emission characteristics of optical bands

Emissivity of optical bands of nano-alumina was evaluated with photoluminescence (PL) spectroscopy. (**Fig. 10 (a), (b),** and **(c)**) show the room temperature PL spectra of the three samples of alumina annealed respectively at temperatures 400, 1000 and 800 ^{0}C. All the samples were excited at a wavelength of 340 nm under identical conditions with a Xenon lamp light source and emission cut filter of 290 nm. It can be seen that the peaks are found at same positions in all the three samples, in the violet and blue band region (at around 410 nm and 450 nm). The most noteworthy change is observed in the PL emission band intensities. The change in intensity may be because of the change in pore size of the material. Increasing pore size offers increasing surface area to the source which causes more absorption of photons and high intensity radiation. The sample corresponding to the annealing temperature of 800 ^{0}C shows the most intense bands, probably due to the presence of large pores. A very recent work has shown that the emissivity of alumina is molded by the presence and in particular the concentration of pores present on the surface [**32**]. It was shown that the emissivity of alumina decreased with increase in pore size and increased as the pores became denser. But the results that we obtained contradict their results to some extent. The energy band gap observed

from photoluminescence spectroscopy is around 3.0 eV in all the three samples. The other emission bands may be because of some defect levels (probably interstitial aluminium) present in the sample. One interesting phenomena is the slight shift that occurs in the spectrum. As we observe from the sample corresponding to 400 ^{o}C annealing temperature to 1000 ^{o}C annealing temperature, the spectra shows slight red shift in the higher wavelength region (for the violet blue bands), but it manifests blue shift in the lower wavelength region (violet bands), although the crystallite sizes showed an upward surge (**Table 1** and **2**). Apparently for the violet bands the effect of crystallite sizes is outweighed by some other factors. Detailed explanation for this anomalous behavior requires further experimental analysis.

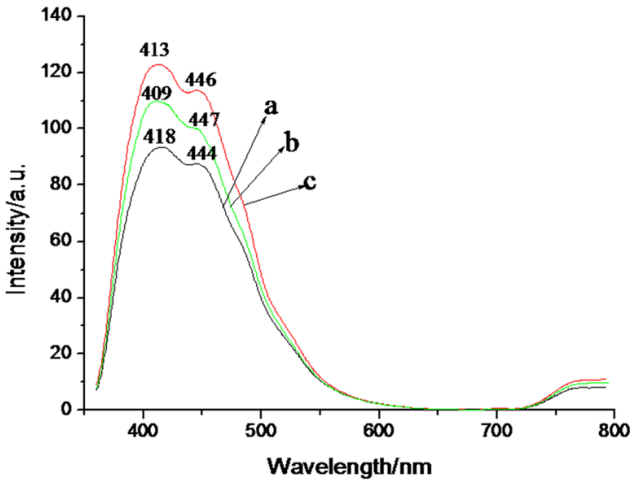

Fig. 10. Photoluminescence spectra of alumina nanoparticles processed under different annealing temperatures; a) 400 ^{0}C b) 1000 ^{0}C c) 800 ^{0}C.

Conclusion

Nanosized alumina powders have been prepared via a simple processing of saturated solutions aluminum nitrate under different annealing conditions. The XRD analysis showed that the complete transformation from γ- Al_2O_3 to α- Al_2O_3 was observed at 1000 ^{0}C. The crystallite size increased with increasing annealing temperature. The resulting α alumina nanopowder exhibits particle agglomerates in the range of 25 to 40 nm in average diameter occur when they annealed at 1000 ^{0}C. Moreover, electron micrographs revealed that on increasing the annealing temperature the material becomes porous. The emission bands were in visible range with violet and blue-violet emissions being prominent. The energy band gap observed from photoluminescence spectroscopy is around 3.0 eV in all the three samples. The synthesis process is remarkably simple, low cost and free of any hazardous instrumentation and to the best of our knowledge has not been reported before. A detailed structure-property correlation has been established for its potential applications.

Acknowledgements

We thank the Director, NPL New Delhi, India for providing the necessary experimental facilities. Dr. N. Vijayen, Dr. S.N. Sharma, Mr. K.N. Sood, Dr. Vijay Totaum are gratefully acknowledged for providing the necessary instrumentation facilities for XRD, FT-IR and SEM and AFM respectively. M/S Carl Zeiss NTS (USA) is gratefully acknowledged for extending the facility of Helium Ion Microscopy to carry out the experiments. One of the authors (AKS) acknowledges CSIR foreign travel grant to visit USA in February 2010. J. Gangwar and K. K. Dey acknowledge the financial support from UGC (Grant No.F.2-61/98 (SA-I)) and CSIR (Grant No.31/001(0325/2009-EMR-I), respectively.

Reference

1. Rai, R. *Adv.Mat.Lett.* **2010**, *1*, 55. **DOI:** 10.5185/amlett.2010.3101
2. Kiri, P.; Hyett, G.; Binions, R. *Adv.Mat.Lett.* **2010**, *1*, 86. **DOI:** 10.5185/amlett.2010.8147
3. Snure, M.; Tiwari, A. *J.Appl.Phys.* **2008**, *104*, 073707. **DOI:** 10.1063/1.2988131
4. Snure, M.; Tiwari, A. *J.Nanosci.NanoTech.* **2007**, *7*, 481. **DOI:** 10.1166/jnn.2007.139
5. Han, D.; Li, Y.; Zia, W. *Adv.Mat.Lett.* **2010**, *1*, 188. **DOI:** 10.5185/amlett.2010.7137
6. Machaka, R.; Mwakikunga, B.W.; Manikandan, E.; Derry, T.E.; Sigalas, L. *Adv.Mat.Lett.* **2011**, *2*, 58. **DOI:** 10.5185/amlett.2010.9167
7. Chen, L.; Pang, X.; Yu, G.; Zhang, J. *Adv.Mat.Lett.* **2010**, *1*, 75. **DOI:** 10.5185/amlett.2010.4117
8. Srivastava, A.K. *Mater.Lett.* **2008**, *62*, 4296. **DOI:** 10.1016/j.matlet.2008.07.09
9. Srivastava, A.K.; Deepa, M.; Sood, K.N.; Erdem, E.; Eichel, R.-A. *Adv.Mat.Lett.* **2011**, *2*, 142. **DOI:** 10.5185/amlett.2011.1201
10. Hass, K.C.; Schneider, W.F.; Curioni, A.; Andreoni, W. *Science*. **1998**, *282*, 265. **DOI:** 10.1126/science.282.5387.265
11. Mchale, J. M.; Auroux, A.; Perrotta, A. J.; Navrotsky, A. *Science.* **1997**, *277*, 788. **DOI:** 10.1126/science.277.5327.788
12. Skrdla, P.J.; Robertson, R.T. *J.Mol.Catal.A:Chemical*. **2003**, *194*, 255. **DOI:** 10.1016/S1381-1169(02)00529-0
13. Sanchez-Valente, J.; Bokhimi, X.; Hern´andez, F. *Langmuir*. **2003**, *19*, 3583. **DOI:** 10.1021/la020423+
14. Temuujin, J.; Jadambaa, T.; Mackenzie, K.J.D.; Angerer, P.; Porte, F.; Riley, F. *Bull.Mater.Sci.* **2000**, *23*, 301.
15. Schaper, H.; Vanreijen, L.L. *Thermochimica Acta.* **1984**, *77*, 383.
16. Levin, I.; Brandon, D. *J.Am.Chem.Soc*. **1998**, *81*, 1995. **DOI:** 10.1111/j.1151-2916.1998.tb02581.x
17. Kureti, S.; Weisweiler, W. *Appl.Catal.A*:Gen. **2002**, *225*, 251.
18. Ichinose, N. Superfine Particle Technology; Springer-Verlag: London, U.K., **1993**.
19. Uyeda, R. *Progress in Materials Science.* **1991**, *35*, 1.
20. Wefers, K.; Misra, C. Oxides and Hydroxides of Aluminium, Technical Paper No. 19; Alcoa, Pittsburg, PA, **1987**.
21. Cottringer et. al, United States Patent, Patent no. 4,623,364; Patent date. November *18*, **1986**.
22. Stierle, A.; Renner, F.; Streitel, R.; Bosch, H.; Brube, W.; Cowie, B.C. *Science.* **2004**, *303*, 1652. **DOI:** 10.1126/science.1094060
23. Huang, C-L.; Wang, J-J.; Huang, F-H. *Mater.Lett.* **2005**, *59*, 3746. **DOI:** 10.1016/j.matlet.2005.06.053
24. Tepper, F.; Kaledin, L., http://www.argonide.com/Paper%20PREP%2007-final.pdf, **2007**.
25. Roy, R. S.; Mitra, M.; Basu, D. *TrendsBiomater.Artif.Organs.* **2005**, *18*, 166.
26. Varatharajan, K.; Dash, S.; Arunkumar, A.; Nithya, R.; Tyagi, A. K.; Raj, B. Mater.Res.Bull. 2003, 38, 577. **DOI:** 10.1016/S0025-5408(03)00026-6
27. Tok, A.I.Y.; Boey, F.Y. C.; Zhao, X. L. *J.Mater.Process.Tech.* **2006**, *178*, 270. **DOI:** 10.1016/j.jmatprotec.2006.04.007
28. Sharma, P. K.; Varadan, V. V. *J.Europ.Ceram.Soc.* **2003**, *23*, 659.
29. Dumeignil, F.; Sato, K.; Imamura, M.; Matsubayashi, N.; Payen, E.; Shimada, H. *Appl.CatalysisA:General.* **2003**, *241*, 319.
30. Qul, L.; He, C.; Yang, Y.; He Y.; Liu, Z. *Mater.Lett.* **2005**, *59*, 4034. **DOI:** 10.1016/j.matlet.2005.07.059
31. Katamreddy, R.; Inman, R.; Jursich, G.; Soulet, A.; Takoudis, C. J.Electro.Chem.Soc. **2006**, *153*, C701.

DOI: 10.1149/1.2239258
32. Kim, B.-N.; Hiraga, K.; Morita, K.; Yoshida, H.; Miyazaki T.; Kagawa, Y. *Acta.Mater.* **2009**, *57*, 1319.
DOI: 10.1016/j.actamat.2008.11.010